Bioconjugate Chemistry

Article

pubs.acs.org/bc

Functionalized Graphene Oxide Nanoparticles for Cancer Cell-Specific Delivery of Antitumor Drug

Xubo Zhao, Liangwei Yang, Xiaorui Li, Xu Jia, Lei Liu, Jin Zeng, Jinshan Guo, and Peng Liu*

State Key Laboratory of Applied Organic Chemistry and Key Laboratory of Nonferrous Metal Chemistry and Resources Utilization of Gansu Province, College of Chemistry and Chemical Engineering, Lanzhou University, Lanzhou 730000, China

ABSTRACT: The unique reduction-triggered functional graphene oxide nanoparticles (GON) with well-defined size and uniform distribution were designed as an innovative drug delivery platform for cancer treatment for the first time, via the redox radical polymerization of methacrylic acid from the polyethylene glycol (PEG) modified GON (GON-PEG), following by cross-linking with cystamine. Thermogravimetric analysis demonstrates that the typical $PMAA_2$-GON-PEG carriers contain about 16 wt % PEG segments and 33 wt % poly(methacrylic acid) (PMAA) brushes. PEG moieties are incorporated to make the drug delivery platforms stealthy during blood circulation. Notably, introducing the cross-linked PMAA brushes efficiently minimizes the premature release of doxorubicin (DOX) in the stimulated normal tissues, and accelerates DOX release in the stimulated tumor tissues through response to reduce agent. The carriers showed a 6-fold faster releasing rate at pH 5.0 in the presence of 10 mM glutathione (GSH) (stimulated tumor tissues) than at pH 7.4 with 10 μM GSH (stimulated normal tissues). In vitro cytotoxicity test also showed that the cross-linked $PMAA_2$-GON-PEG ($CPMAA_2$-GON-PEG) carriers had remarkable cytocompatibility, and that the DOX-loaded $CPMAA_2$-GON-PEG had excellent killing capability to SiHa cells.

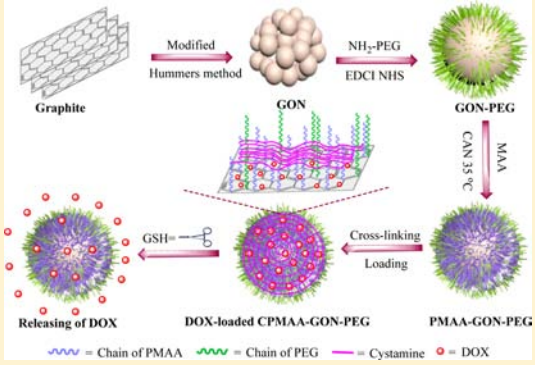

INTRODUCTION

Among various nanomaterials, the development in graphene-based materials in the past decade is like a modern fairy tale of how an ugly cygnet transforms into a white swan. Andre Geim and co-workers' first discovery of graphene has broken new ground in material and condensed matter physics.[1,2] Owing to its remarkably unique Young's modulus, mobility of charge carriers, electronic and thermal properties, fracture strength, specific surface area, and biocompatibility,[3] graphene has become a promising frontier in chemical and physical applications, such as electronics, optoelectronic devices, and photoconductive materials in solar cells to medical imaging, drug delivery, and tissue engineering.[4]

With developments in nanobiotechnology, novel graphene-based nanomaterials have rapidly grown and shown great potential as an attractive candidate in imaging, photothermal therapy, bacterial inhibition, drug delivery, and biosensor development.[5−10] It is extremely important that the graphene-based nanomaterials should be nontoxic, water-dispersible, and biocompatible for biomedical applications.[11] The biomedical research on functional graphene oxide (GO) has been attracting a great deal of attention recently. Starting from 2008, numerous attempts have been made to optimize the GO properties to win the war against cancer. Liu's groups studied the pharmacokinetics and biodistribution of graphene using radionuclide labeled PEGylated graphene and carried out a systemic toxicology examination of functionalized graphene in mice.[12] Recently, Wang and co-workers reported a novel SiO_2-coated quantum dot (HQDs)-conjugated graphene to deliver DOX to the targeted cancer cells, localize the graphene-based HQDs, and monitor the intracellular DOX release.[13]

In spite of these advantages for engineered nanocarriers as a drug delivery platform, they face several challenges including the programmed release of drugs, stability, and site-specific delivery for medical application.[14] Considering these drawbacks of drug delivery systems (DDS), in the anti-cancer war, one of the main obstacles is severe toxic side effects of anticancer drugs to normal tissues, due to the premature release of drugs during blood circulation, and overcoming capture by the reticuloendothelial system (RES).[15] Thus, it is extremely important that nanovehicles with extended blood circulation duration favor tumor accumulation via the EPR effect, as well as minimize the premature anticancer drug release during blood circulation. Compared with normal tissues, tumor tissues possess a variety of unique microenvironmental features and physicochemical properties, including weak acidity,[16] abnormal temperature gradients,[17] overexpressed proteins and enzymes,[18] and others. Most importantly, the intracellular microenvironments of the tumor tissues are drastically different from those of normal tissues: acidic pH inside endosomes and lysosomes (pH 5.0−5.5);[19] reductive microenvironments due to high level cysteine or glutathione (GSH) in the cytoplasm and endolysosomes.[20] These could be utilized to modulate the release of the anticancer drug loading.

Received: November 9, 2014
Revised: December 17, 2014
Published: December 19, 2014

DOI: 10.1021/bc5005137
Bioconjugate Chem. 2015, 26, 128−136

Scheme 1. Schematic Illustration of the Preparation, Ideal Structural Transformation, Drug Loading, and Reduction-Triggered Release of the CPMAA-GON-PEG Carriers

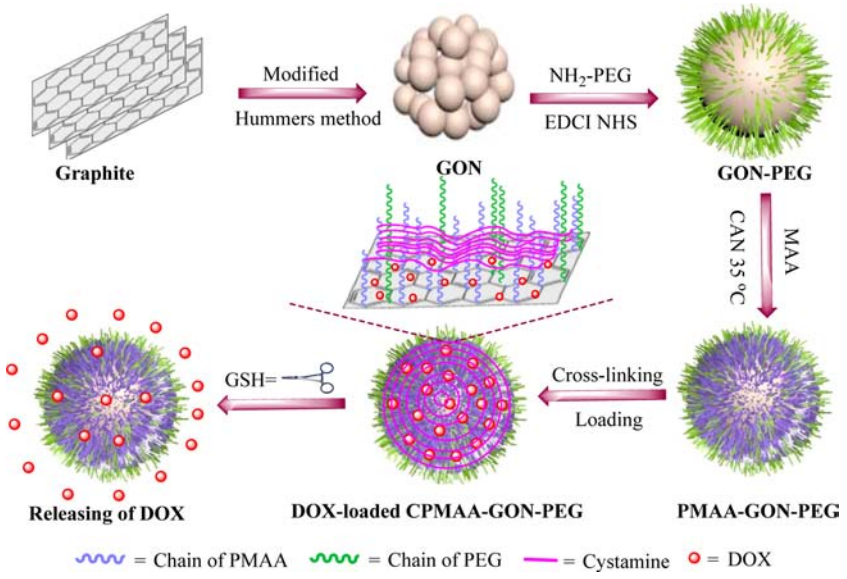

To utilize these differences between tumor tissues and normal tissues, numerous efforts and studies were undertaken to boost the application of functional graphene-based materials for cancer therapy.[21] For examples, Cui's group utilized a graphene oxide base with redox-response to efficiently regulate DOX release under a GSH regulated reducing environment.[22] Shi and co-workers successfully prepared the triple stimuli-responsive graphene oxide-based nanotheranostics to reverse the multidrug resistance (MDR) of cancer cells through loading of anticancer drug and significantly inhibit the metastasis of cancer cells by down-regulating the expression of metastasis-related proteins.[23] In addition, Liu and workmates provided the nanographene oxide-based nanocarriers with smart pH-response for combining photothermal and chemical therapy to overcome drug resistance in response to the external physical stimulus and tumor microenvironment.[24] Recently, our group also reported novel functional graphene oxide nanoparticle (GON)-based nanocarriers to deliver anticancer drug (DOX) under stimuli-response of the tumor microenvironment.[25]

To overcome the above drawbacks for anticancer DDS, novel graphene-based DDS was designed with the PEGylated GON as drug carriers and the disulfide bond-cross-linked PMAA brushes as reduction-triggering switch in the present work (Scheme 1). The typical CPMAA$_2$-GON-PEG carriers, which are chosen as the desired DDS through a series of optimizing experiments, have several important designing aspects: (i) the versatile drug delivery platform with grafted PEG moieties must be endowed biocompatibility and water-dispersion; (ii) it possesses reduction-triggered switching characteristic in intracellular microenvironments of tumor tissues due to the introduction of disulfide cross-linking bond (−S−S−); (iii) the premature release of the encapsulated doxorubicin could be avoided in normal tissues, while the release could be accelerated in tumor tissues. To demonstrate the feasibility of the fabrication process, herein, the transmission electron microscope (TEM) image, Fourier transform infrared (FT-IR) spectroscopy analysis, thermogravimetric analysis (TGA), dynamical light scattering (DLS) measurements, WST-1 assays, as well as in vitro drug loading and release experiments were investigated.

RESULTS AND DISCUSSION

Fabrication of CPMAA-GON-PEG. The fabrication approach for the biocompatible and reduction-responsive CPMAA-GO-PEG nanocarriers is presented in Scheme 1, via the classic amidation of the carboxyl groups of the GON nanoparticles with the amine end-groups of the functional poly(ethylene glycol) (PEG), and the radical polymerization of MAA initiated with the redox system of cerium ammonium nitrate (CAN)/the active hydrogen atoms of the GON-PEG nanoparticles (Table 1),[26−28] and finally the cross-linking of the

Table 1. Redox Radical Polymerizing Conditions

samples	MAA (mmol)	CAN (mmol)
PMAA$_1$-GON-PEG	11.5	0.2887
PMAA$_2$-GON-PEG	23.0	0.2887
PMAA$_3$-GON-PEG	34.5	0.2887

PMAA brushes with cystamine as a cross-linker (Table 2), to endow the PMAA-GON-PEG with reduction responsiveness in the presence of high level cysteine or glutathione (GSH) in the cytoplasm and endolysosomes.[29]

Table 2. Cross-Linking Conditions

samples	MAA[a] (mmol)	Cys (mg)	EDCI (mg)	NHS (mg)
PMAA$_1$-GON-PEG	1.28	28.82	49.07	29.46
PMAA$_2$-GON-PEG	3.83	86.24	146.84	88.15
PMAA$_3$-GON-PEG	5.45	122.73	208.95	125.45

[a]The molar content of MAA per gram of the PMAA-GON-PEG nanoparticles was calculated by TGA.

After the PEGylation with NH$_2$−PEG, the characteristic absorbance at 1720 cm^{-1} of the carbonyl band in carboxylic acid disappeared, while the new absorbance at 1650 cm^{-1} of the carbonyl band in amide group and the characteristic peak at 1110 cm^{-1} of the oxygen stretching vibration of the C−O−C group appeared (Figure 1). Furthermore, the C−H stretch peaks around 2900 cm^{-1} were obviously enhanced. It revealed

DOI: 10.1021/bc5005137
Bioconjugate Chem. 2015, 26, 128−136

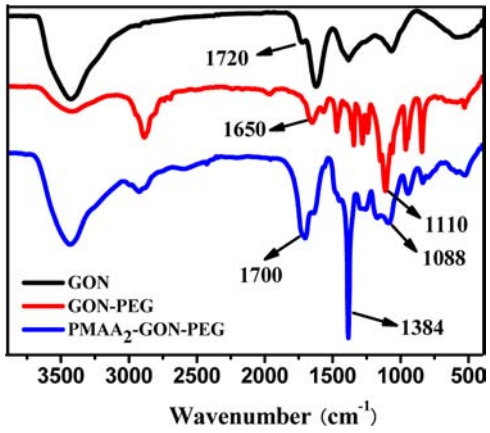

Figure 1. FT-IR spectra of the GON, GON-PEG, and $PMAA_2$-GON-PEG nanoparticles measured in KBr pellets.

that the PEG brushes had been successfully modified onto the GON nanoparticles via amidation. As for the typical $PMAA_2$-GON-PEG nanoparticles, the strong characteristic absorbance peak at 1384 cm^{-1} of the methyl group of PMAA appeared. The characteristic absorbance of the carbonyl band in carboxylic acid and the oxygen stretching vibration of the C−O−C group appeared at 1700 and 1088 cm^{-1}, respectively. The reappearance of the carbonyl band in carboxylic acid was attributed to the grafted PMAA brushes, and the shifts in the two peaks resulted from the hydrogen bond formed between the two functional groups.[30]

TGA technique was utilized to evaluate the contents of the PMAA and PEG brushes grafted onto the GON nanoparticles (Figure 2). All the samples exhibited small mass loss of about 3

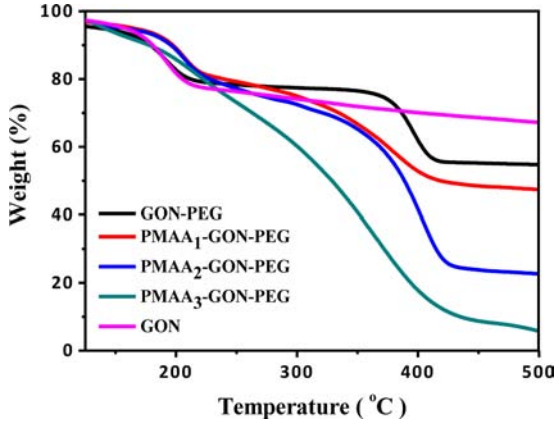

Figure 2. TGA curves of the GON, GON-PEG, $PMAA_1$-GON-PEG, $PMAA_2$-GON-PEG, and $PMAA_3$-GON-PEG nanoparticles at a heating rate of 10 °C min^{-1} in nitrogen.

wt % upon heating even below 100 °C, attributed to the release of moisture. For the GON nanoparticles, the main mass loss occurred around 200 °C due to the pyrolysis of the labile oxygen-containing groups.[31] The TGA data for the GON-PEG, $PMAA_1$-GON-PEG, $PMAA_2$-GON-PEG, and $PMAA_3$-GON-PEG nanoparticles showed a weight loss of 42%, 55%, 78%, and 92% upon 450 °C, respectively, whereas the GON nanoparticles had only a weight loss of 22%. Therefore, it could be calculated that the GON-PEG nanoparticles contained about 16% PEG segment, and that the $PMAA_1$-GON-PEG, $PMAA_2$-GON-PEG, and $PMAA_3$-GON-PEG nanoparticles contained 10%, 33%, and 47% PMAA brushes, respectively. These results demonstrated that the PMAA degree of grafting of the PMAA-GON-PEG nanoparticles could be easily controlled by adjusting the redox radical polymerizing conditions.

The morphology and size of the GON, GON-PEG, and PMAA-GON-PEG nanoparticles were tracked by TEM (Figure 3). The GON nanoparticles showed nearly spherical shape and

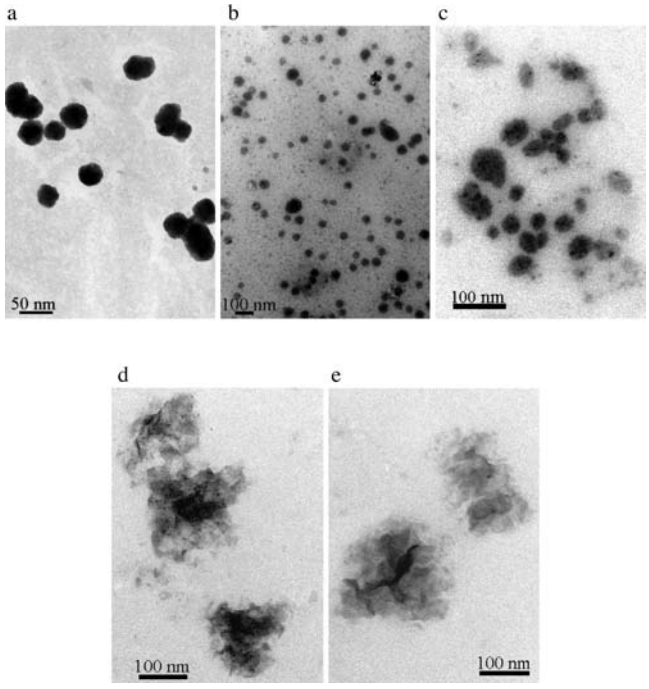

Figure 3. TEM images of the GON (a), GON-PEG (b), $PMAA_1$-GON-PEG (c), $PMAA_2$-GON-PEG (d), and $PMAA_3$-GON-PEG (e) nanoparticles.

near-monodisperse size, with a diameter of approximately 40 nm (Figure 3a). After the PEGylation to provide the desired biocompatibility, the GON-PEG nanoparticles had similar diameter to the GON nanoparticles and the aggregates had been obviously reduced (Figure 3b). With increase of the grafting degree of the PMAA brushes, the GON nanoparticles unfolded and the particle size increased to 70, 110, and 180 nm for the $PMAA_1$-GON-PEG, $PMAA_2$-GON-PEG, and $PMAA_3$-GON-PEG nanoparticles (Figure 3c,de), respectively. With more PMAA brushes grafted, the GON in the $PMAA_2$-GON-PEG and $PMAA_3$-GON-PEG nanoparticles were unfolded more obviously to nonspherical morphology.

Furthermore, the morphological analysis of the GON, GON-PEG, and $PMAA_2$-GON-PEG was carried out with the SEM technique. The GON nanoparticles exhibited a well-defined 3-dimensional structure with a unique diameter of nearly 40 nm (Figure 4a). Interestingly, the diameter of the GON-PEG increased to around 60 nm via PEGylation (Figure 4b). The difference between SEM and TEM images was likely due to the particle size distribution. More importantly, the $PMAA_2$-GON-PEG showed folding and rough surface and dense polymer structure (Figure 4c), consistent with the TEM results. With the above results taken into consideration, PEGylation of GON and modification of PMAA moieties were successful.

Owing to the introduction of PEG segments and PMAA brushes, the $CPMAA_2$-GON-PEG nanoparticles have outstanding dispersion stability in aqueous dispersion and PBS

DOI: 10.1021/bc5005137
Bioconjugate Chem. 2015, 26, 128−136

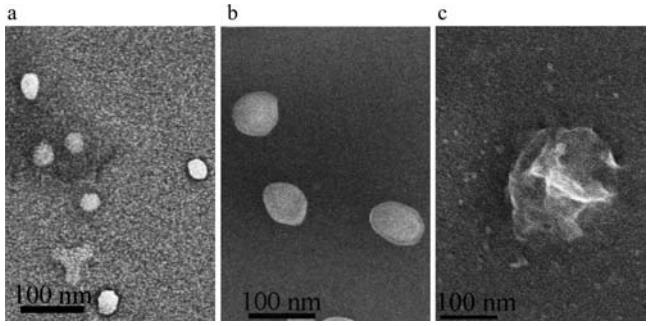

Figure 4. SEM images of GON (a), GON-PEG (b), and $PMAA_2$-GON-PEG (c).

(pH 7.4 or 5.0) dispersion. As shown in Figure 5, the $CPMAA_2$-GON-PEG nanoparticles were stably dispersed in aqueous

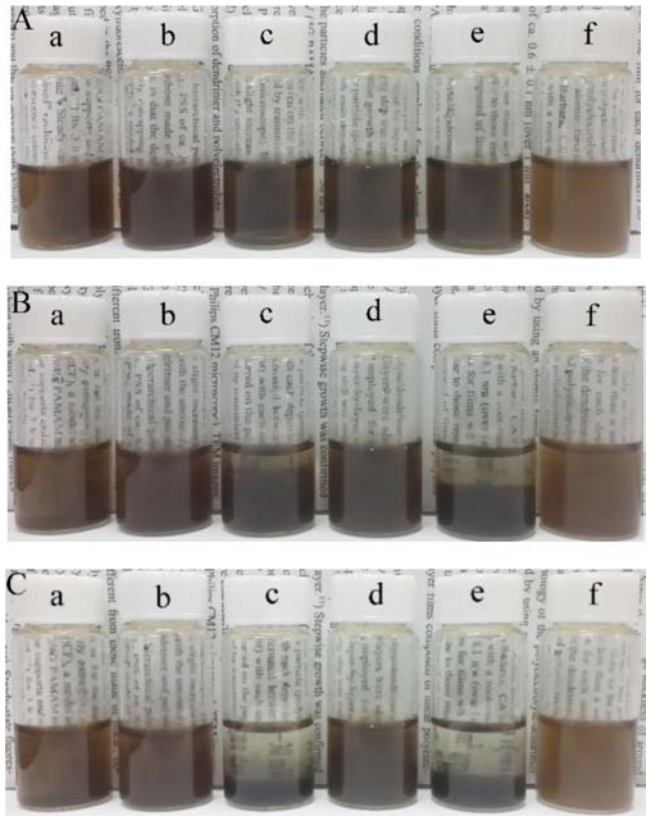

Figure 5. Digital photographs of the dispersion status of the GON in (a) aqueous solution (pH 7.0), (c) PBS (pH 7.4), and (e) PBS (pH 5.0) and the $CPMAA_2$-GON-PEG in (b) aqueous solution (pH 7.0), (d) PBS (pH 7.4), and (f) PBS (pH 5.0), respectively, for different dispersion times of (A) 0 min, (B) 26 min, and (D) 24 h. The concentration of an equivalent dose of GON in all samples was around 0.20 mg mL^{-1}.

dispersion and PBS (pH 7.4 and 5.0) in the range of time from 0 to 26 min or over a long time. However, the GON nanoparticles quickly precipitated after sonication in PBS was stopped (pH 7.4 and 5.0) within 26 min. A similar phenomenon was also reported previously.[11,25,32]

The $PMAA_2$-GON-PEG nanoparticles were then chosen for the biocompatible and reduction-responsive drug carriers due to their compromising degree of grafting of PMAA brushes and particle size, by cross-linking the PMAA brushes with cystamine. The cross-linked PMAA layers on the designed drug carriers ($CPMAA_2$-GON-PEG nanoparticles) are expected to prevent the premature drug release in the circulatory system. The average hydrodynamic diameter (D_h) of the GON, GON-PEG, $PMAA_2$-GON-PEG, and $CPMAA_2$-GON-PEG nanoparticles at pH 7.4 were tracked using DLS measurements (Figure 6). All these nanoparticles displayed narrow unimodal

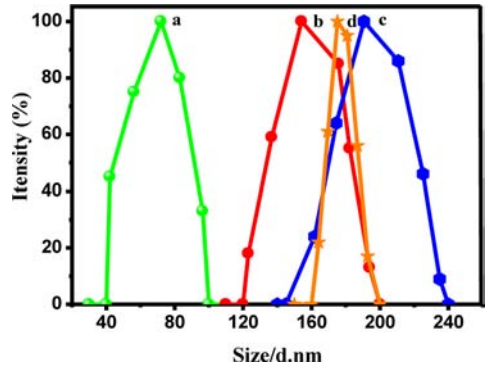

Figure 6. Typical average hydrodynamic diameter distributions of the GON (a), GON-PEG (b), $PMAA_2$-GON-PEG (c), and $CPMAA_2$-GON-PEG nanoparticles (d).

size distribution with D_h of 72, 154, 191, and 175 nm, respectively. With the grafting of PEG and PMAA brushes, the D_h increased, while it decreased after the cross-linking of the PMAA brushes. The D_h of 175 nm of the $CPMAA_2$-GON-PEG nanoparticles at pH 7.4 could ensure the passive targeting function of the drug carriers via the EPR effect.

Drug Loading and Triggered Release. The drug-loading capacity (DLC) and drug-loading efficiency (DLE) of the three cross-linked drug carriers ($CPMAA_1$-GON-PEG, $CPMAA_2$-GON-PEG, and $CPMAA_3$-GON-PEG) were measured as 0.487 ± 0.01, 0.430 ± 0.013, and 0.266 ± 0.014 mg mg^{-1}, and 48.74 ± 0.8%, 42.96 ± 1.3%, and 26.58 ± 1.4% in pH 7.4 at room temperature for DOX, respectively. These values were distinctly lower than those of the GON nanoparticles (0.978 ± 0.012 mg/mg and 97.8% ± 1.2%). This finding also demonstrated that the aromatic graphene oxide sheets had been coated with thicker cross-linked PMAA layers in the CPMAA-GON-PEG nanoparticles, with increased amount of the PMAA brushes grafted from the $CPMAA_1$-GON-PEG to the $CPMAA_3$-GON-PEG, leading to the decrease in the DLC and DLE of DOX via the $\pi-\pi$ stacking interaction.[33]

Compared with significant fluorescence quenching for the DOX-loaded $CPMAA_2$-GON-PEG in deionized water, the fluorescence was recovered when the dispersed medium was transferred from deionized water to ethanol (Figure 7). It is noted that the fluorescence quenching of DOX is caused by the photoinduced electron-transfer effect from the loading process.[34] The clear difference in deionized water and ethanol demonstrated that DOX was successfully loaded onto the $CPMAA_2$-GON-PEG carriers.

The higher DLC and DLE of the un-cross-linked $PMAA_2$-GON-PEG nanoparticles for DOX were measured as 0.574 ± 0.009 mg mg^{-1} and 57.34 ± 0.9% under the same drug-loading condition respectively, higher than those of the $CPMAA_2$-GON-PEG nanoparticles. This resulted from the DOX-loaded onto the PMAA brushes via the electrostatic interaction. It also revealed that the polymer brushes in the $CPMAA_2$-GON-PEG nanoparticles had been successfully cross-linked.

DOI: 10.1021/bc5005137
Bioconjugate Chem. 2015, 26, 128−136

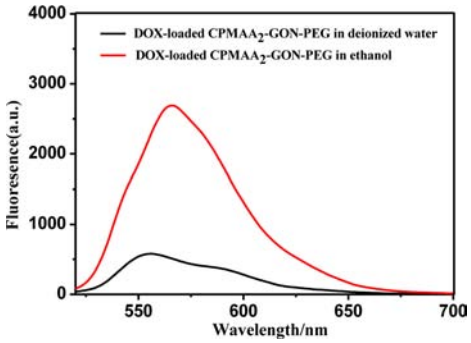

Figure 7. Fluorescence spectra of the DOX-loaded $CPMAA_2$-GON-PEG in deionized water and ethanol with concentration of around 2.5×10^{-4} mg mL^{-1}.

The controlled releasing performance of the DOX-loaded different platforms of the CPMAA-GON-PEG nanoparticles was investigated at 37 °C under pH 5.0 in the absence or presence of 10 mM GSH. As presented in Figure 8, the DOX cumulative release from the $CPMAA_1$-GON-PEG, $CPMAA_2$-GON-PEG, and $CPMAA_3$-GON-PEG nanoparticles was 45.31%, 45.89%, and 32.19% at pH 5.0 after 60 h in the absence of GSH, and 48.46%, 66.48%, and 70.63%, at pH 5.0 after 60 h in the presence of 10 mM GSH, respectively. The high difference in the cumulative DOX release from the DOX-loaded $CPMAA_2$-GON-PEG nanoparticles demonstrated that the cross-linked PMAA layers in the $CPMAA_2$-GON-PEG nanoparticles could efficiently provide the desired reduction-stimuli-responsive controlled release characteristics, besides their smaller particle size and higher DLC and DLE.

The extracellular pH and GSH level in the normal tissues and blood is approximately 7.4 and 10 μM, respectively, whereas the average pH is 5.0−5.5 and the GSH level is up to 10 mM inside endosomes and lysosomes in the extracellular tumor tissues. Considering these differences, the in vitro controlled release of DOX from the DOX-loaded $CPMAA_2$-GON-PEG carriers was also investigated at 37 °C under different media, i.e., (i) pH 7.4 without GSH, (ii) pH 7.4 with 10 μM GSH, and (iii) pH 7.4 with 10 mM GSH, as shown in Figure 8c. The DOX cumulative release from the $CPMAA_2$-GON-PEG carriers was about 9.09% at pH 7.4 after 60 h in the absence of GSH. In the presence of 10 μM GSH, which confirmed the stability of the $CPMAA_2$-GON-PEG carriers and a low premature drug release in a physiological pH and GSH (mimicking the normal tissue), the DOX cumulative release was 11.32% on the same time scale, while that from the un-cross-linked $PMAA_2$-GON-PEG nanoparticles was found to be 23.53% (Figure 8d). By increasing the concentration of GSH to 10 mM, the cumulative release of DOX increased to 25.72%. This result showed that the $CPMAA_2$-GON-PEG carriers might prevent the theft of DOX from the DOX-loaded $CPMAA_2$-GON-PEG carriers. In addition, the cumulative release ratio of DOX was significantly accelerated at pH 5.0 as 45.29% in 60 h, likely due to that the decreasing pH value weakening the $\pi-\pi$ stacking interaction

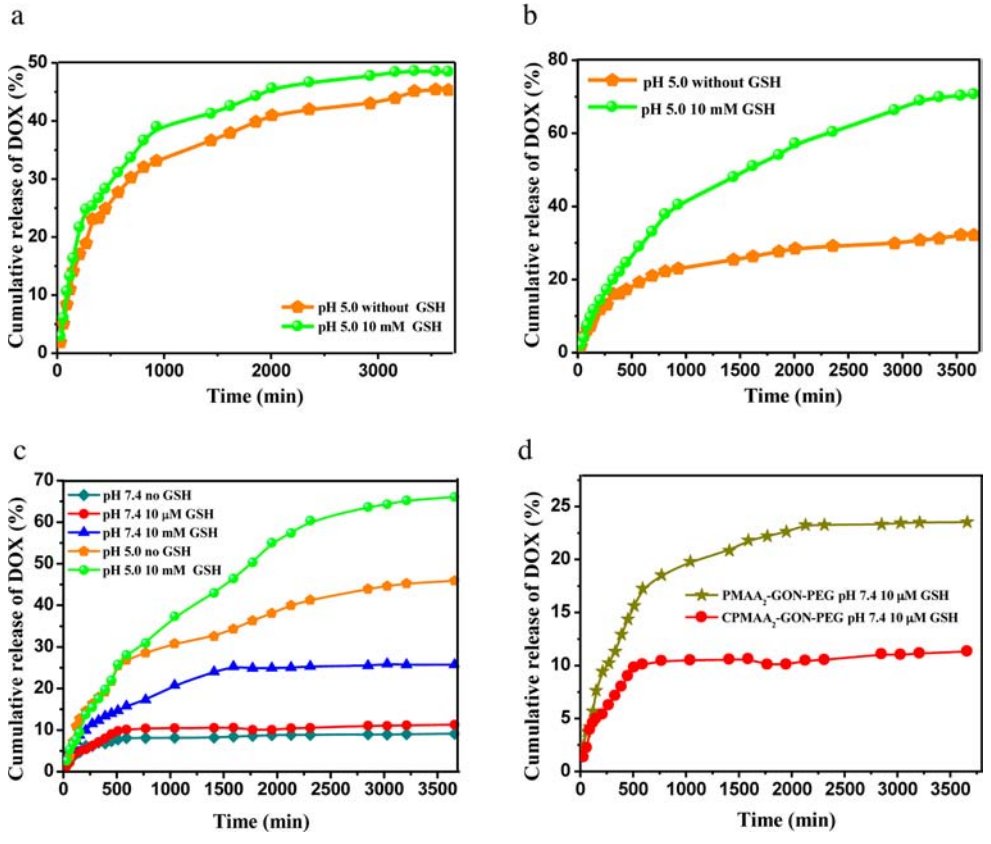

Figure 8. Cumulative DOX release from (a) the DOX-loaded $CPMAA_1$-GON-PEG nanoparticles and (b) $CPMAA_3$-GON-PEG nanoparticles in PBS (pH 5.0) without or with 10 mM GSH at 37 °C, (c) the DOX-loaded $CPMAA_2$-GON-PEG nanoparticles in PBS at 37 °C (pH 7.4 without GSH), (pH 7.4 with 10 μM GSH), (pH 7.4 with 10 mM GSH), (pH 5.0 without GSH) and (pH 5.0 with 10 mM GSH), and (d) the DOX-loaded $PMAA_2$-GON-PEG and $CPMAA_2$-GON-PEG nanoparticles at PBS (pH 7.4) with 10 μM GSH at 37 °C, respectively.

DOI: 10.1021/bc5005137
Bioconjugate Chem. 2015, 26, 128−136

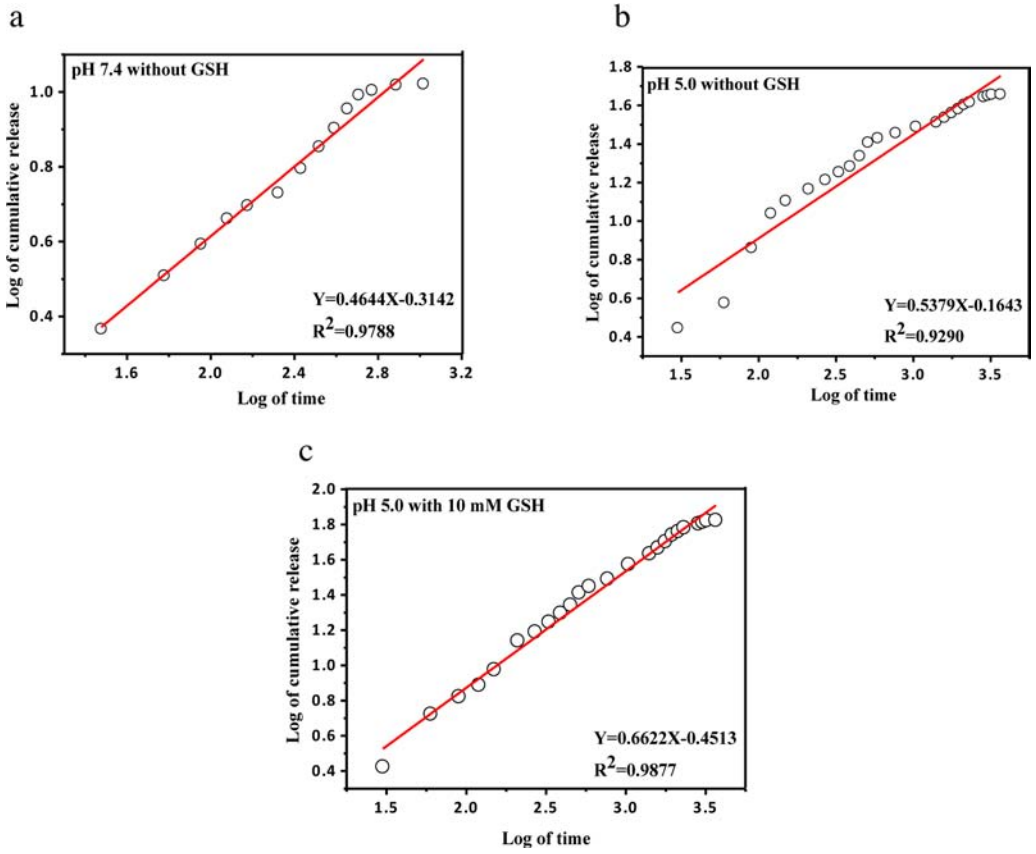

Figure 9. Curves of Korsmeyer-Peppas models for the drug release from DOX-loaded CPMAA$_2$-GON-PEG carriers under different conditions: (a) pH 7.4, (b) pH 5.0, and (c) pH 5.0 with 10 mM GSH.

between that aromatic network of the platform and DOX, due to its acidic solubility.

In order to simulate the intracellular trafficking process, drug release were performed at pH 5.0 with 10 mM GSH (mimicking the acidic endosomal compartments). The cumulative release was 66.48% within 60 h. The in vitro drug release profiles presented in Figure 8c demonstrated that the initial DOX release was 6-fold faster at pH 5.0 in the presence of 10 mM than at pH 7.4 in the presence of 10 μM GSH.

More importantly, the total amount of DOX released from the CPMAA$_2$-GON-PEG carriers apparently increased under acidic conditions and GSH (11.32 wt % at pH 7.4 in the presence of 10 μM GSH, 25.72 wt % at pH 7.4 in the presence of 10 mM GSH, 45.29 wt % at pH 5.0 in the absence of GSH, and 66.48 wt % at pH 5.0 in the presence of 10 mM GSH, respectively). This results demonstrated that the premature release of DOX during blood circulation could be minimal due to the favorable stability of the cross-linked polymer layers at pH 7.4 in the presence of 10 μM GSH. Consequently, patients are expected to greatly benefit from reduction in severe toxic side effects of anticancer drugs to normal tissues. Furthermore, this strongly supports our hypothesis that the apparent release of DOX in stimulated tumor tissues might be maximized by cleaving the disulfide bridge bond in the cross-linked PMAA layers and increasing acidity. Therefore, these results clearly indicate that reduction and pH stimulus-responsive biocompatible CPMAA$_2$-GON-PEG carriers present synergistic effects in DOX release, namely, the tumor microenvironment-responsive triggered release performance. Notably, DOX could be effectively released in the presence of elevated GSH.

The semiempirical Korsmeyer-Peppas equation was utilized to fit the accumulative release data and the coefficients of correlation (R^2) were used to evaluate the fitting accuracy at pH 7.4 without GSH, pH 5.0 without GSH, or pH 5.0 with 10 mM GSH at 37 °C (Figure 9). The plots for the Korsmeyer-Peppas equation for the DOX-loaded CPMAA$_2$-GON-PEG carriers resulted in linearity with R^2 and n values of 0.9788 and 0.4644, 0.9290 and 0.5379, and 0.9877 and 0.6622, respectively. It yields comparatively good linearity with release exponents (n) of approximately 0.5. This suggested that the release mechanism of DOX fitted the Fickian diffusion at pH 7.4 without GSH.[35] In contrast, the n values at other releasing conditions were found to be 0.5379 and 0.6622, showing that the transport process of DOX was anomalous, corresponding to a pseudo-Fickian or Case III mechanism,[35,36] considering the cutting off of the disulfide bridge bonds of the CPMAA$_2$-GON-PEG carriers, which promotes the cumulative release of DOX at pH 5.0 in the presence of 10 mM GSH. Meantime, the n value was 0.5379 at pH 5.0, the anomalous diffusion was considered so that the release of DOX was accelerated in slightly acidic condition mimicking the tumor microenvironment. Simultaneously, the compact cross-linked polymer layers hindered the diffusion of DOX, compared to the release mechanism at pH 5.0 in the presence of 10 mM GSH.

Toxicity and Cell-Killing Activity for SiHa and LSECs Cells. Feasibility of biocompatibility of drug delivery platform (CPMAA2-GON-PEG) and cell killing with this novel reduction and pH responsive DOX-loaded drug delivery platform (DOX-loaded CPMAA$_2$-GON-PEG) was assessed by WST-1 assays for SiHa cells (the acervical squamous cancer

DOI: 10.1021/bc5005137
Bioconjugate Chem. 2015, 26, 128−136

cells and generally accepted in vitro model of parenchymal cells in the liver, hepatocytes[37]) and LSECs (a normal cell). As shown in Figure 10, the CPMAA$_2$-GON-PEG nanocarriers

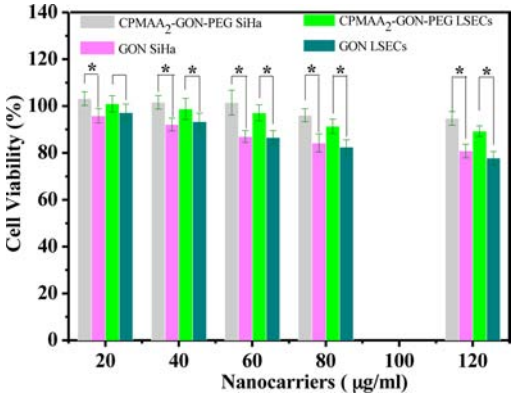

Figure 10. Biocompatibility of the CPMAA$_2$-GON-PEG and GON were determined by standard WST-1 assay. Data are presented as the mean ± standard deviation (SD; $n = 6$). The asterisks indicate $P < 0.01$ between the two groups. When the P value was less than 0.01, differences were considered statistically significant.

were reasonably safe up to 120 μg mL^{-1} (cell viability >97%) for all the testing concentrations after 48 h of incubation, indicating that the CPMAA$_2$-GON-PEG nanocarriers had little toxicity on not only SiHa cells, but also LSECs in the given concentration range, in comparison with the GON. Furthermore, with the increase of concentration of the GON and CPMAA$_2$-GON-PEG nanocarriers, results were statistically significant, as shown in Figure 10. These results demonstrate that the functionalization of GON is extremely essential for biomedical application.

The therapeutic efficacy of the DOX-loaded CPMAA$_2$-GON-PEG in the absence or presence of GSH-OEt and free DOX for SiHa cell, and the DOX-loaded CPMAA$_2$-GON-PEG and free DOX for LSECs cell, were also compared in Figure 11. Free DOX alone significantly reduced the viability of SiHa cells and

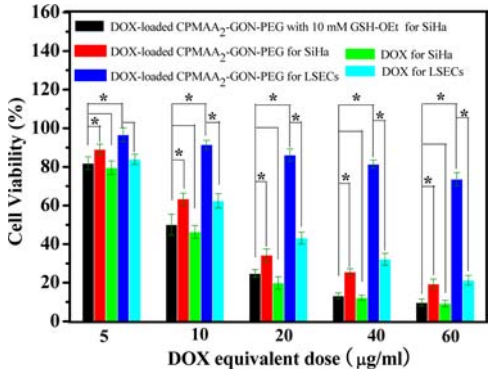

Figure 11. Antitumor activity of the DOX-loaded CPMAA$_2$-GON-PEG in the presence or absence of 10 mM GSH-OEt for SiHa cells, free DOX as a function of DOX dosages determined by standard WST-1 assay. In addition, cytotoxicity of the DOX-loaded CPMAA$_2$-GON-PEG for the normal cell (LSECs) was measured under the same conditions. Data are presented as the mean ± standard deviation (SD; $n = 6$). The asterisks and triangles indicate $P < 0.01$ between the two groups and various concentrations in the same group, respectively. When the P value was less than 0.01, differences were considered statistically significant.

LSECs in the tested concentration range. More importantly, the DOX-loaded CPMAA$_2$-GON-PEG nanoparticles do not significantly affect proliferation of LSECs (a normal cell) up to a concentration of 40 μg mL^{-1} (the cell-killing activity was 81.38%), as shown in Figure 11. In addition, the DOX-loaded CPMAA$_2$-GON-PEG nanoparticles have similar cell-killing activity to free DOX in a dose-dependent manner. Meantime, the cell-killing activity of DOX-loaded CPMAA$_2$-GON-PEG nanocarriers in the presence of 10 mM GSH-OEt was higher than that in the absence of GSH. Finally, with the increase of DOX equivalent concentration of the DOX-loaded CPMAA$_2$-GON-PEG from 40 to 60 μg mL^{-1}, results were not statistically significant (Figure 11). The reason was potentially that 40 μg mL^{-1} of DOX equivalent concentration was enough to inhibit viability of the SiHa cells. From the discussion above, it could be concluded that the functional GON nanoparticles had excellent biocompatibility and were developed to sense reduction/pH variations that differentiate cancer cells from normal cells.

CONCLUSIONS

An innovative method has been developed for synthesizing unique reduction/pH dual sensitive graphene oxide nanoparticle (GON)-based drug carriers with well-defined size and uniform distribution via the PEGylation and grafting PMAA brushes via redox radical polymerization, followed by cross-linking with cystamine. The CPMAA$_2$-GO-PEG nanoparticles with the middle degree of grafting of the PMAA brushes were chosen as the desired drug delivery system through optimization experiments. The results demonstrated that the versatile drug delivery platform possessed biocompatibility and reduction/pH stimulus-responsive properties toward the tumor microenvironments. For the encapsulated doxorubicin (DOX), the premature release could be minimal during blood circulation, while it was maximized in tumor tissues via the EPR effect by the tumor microenvironment-triggered accelerated release. Consequently, this novel drug delivery platform is expected to appear brilliantly promising for cancer treatment.

EXPERIMENTAL SECTION

Materials. Graphite powder was purchased from Huatai Chemical Reagent Co. Ltd. Monofunctional PEG (NH_2–PEG_{2000}) was provided by Beijing Kaizheng Biological Engineering Development Co. Ltd.

Cystamine dihydrochloride (Cys, 98%) was provided by J&K Chemical Ltd. 1-Ethyl-3-(3-dimethyl aminopropyl) carbodiimide hydrochloride (EDCI) was purchased from Fluorochem. *N*-Hydroxylsuccinimide (NHS) was purchased from Aladdin Chemistry Co. Ltd. Doxorubicin hydrochloride (DOX) was purchased from Beijing Huafeng United Technology Co. Ltd. All other reagents were of analytical reagent grade from Tianjin Chemical Company without further purification. Deionized water was used throughout the experiments.

PEGylation of GON. The three-dimensional (3D) graphene oxide nanoparticles (GON) were synthesized referring to a modified Hummers method with natural graphite powder as the raw material.[25,38]

The GON dispersion was diluted with water to 200 mL with solid content of about 1 mg mL^{-1}. After it was ultrasonicated with 20 mg mL^{-1} NH_2–PEG for 15 min, EDCI (5 mM) was added and the dispersion was ultrasonicated for another 30 min, followed by adding enough EDCI to reach 20 mM and

DOI: 10.1021/bc5005137
Bioconjugate Chem. 2015, 26, 128−136

stirring for 12 h. The final product was centrifuged and washed with water to remove any excess free NH_2−PEG. The PEGylated GON (GON-PEG) nanoparticles were freeze−dried and stored at 4 °C.

Redox Radical Polymerization of MAA from GON-PEG. The PMAA brushes were grafted from the surface of the GON-PEG by the redox radical polymerization technique with cerium ammonium nitrate (CAN) as oxidant.[26] Typically, 200 mL 2 mg mL^{-1} GON-PEG aqueous dispersion was prepared by ultrasonicating for 30 min, then MAA was added. CAN in 1.0 mol L^{-1} nitric acid solution was then added into the GON-PEG dispersion dropwise for 3 min. During the entire preparation process, the mixture was electromagnetically stirred at 35 °C for 6 h under nitrogen atmosphere. Different feeding ratios of MAA were utilized to modify the GON-PEG in order to obtain the desired products along with the same concentration of initiator CAN as presented in Table 1. After the grafting polymerization, the product was separated by centrifugation at 12 000 rpm for 15 min, and the sediment was washed with water to remove the excess monomer and the possible free, ungrafted polymer. The resultant products (PMAA-GON-PEG) were collected and dried under vacuum at 35 °C to constant weight.

Cross-Linking PMAA-GON-PEG with Cystamine. To endow reduction-response of the PMAA-GON-PEG nanoparticles, cystamine (Cys) was utilized to cross-link the PMAA moieties, with the molar ratio of cystamine to the total carboxyl groups in the PMAA-GON-PEG nanoparticles of 1:2 (Table 2). The PMAA-GON-PEG was dispersed into 100 mL phosphate buffered saline (PBS, pH 7.4) until about 2 mg mL^{-1}. It was then ultrasonicated with 0.5 equiv of Cys for 30 min. One equivalent of EDCI and NHS was afterward added to the mixture. The solution was sonicated for another 30 min, and then magnetically stirred for 24 h. The products were centrifuged and washed with deionized water to remove any excess Cys. The obtained cross-linked PMAA-GON-PEG (CPMAA-GON-PEG) nanoparticles were freeze−dried and stored at 4 °C.

Drug-Loading and Triggered Release. Drug-loading and release of the CPMAA-GON-PEG, PMAA-GON-PEG, and GON were performed as in previous work.[25] 10.0 mg samples of the drug carriers were dispersed into 10.0 mL of 1.0 mg mL^{-1} DOX solution at pH 7.4 for the DOX-loading.

Different typical conditions (at pH 7.4 without GSH, pH 7.4 with 10 μM GSH, pH 7.4 with 10 mM GSH, pH 5.0 without GSH, and pH 5.0 with 10 mM GSH) were used to investigate the DOX release from the DOX-loaded $CPMAA_2$-GON-PEG. To compare with the DOX-loaded $CPMAA_2$-GON-PEG, the drug release performance of the DOX-loaded $CPMAA_1$-GON-PEG and DOX-loaded $CPAMA_3$-GON-PEG was evaluated in PBS (pH 5.0 without GSH, and pH 5.0 with 10 mM GSH), and that of the DOX-loaded non-cross-linked $PMAA_2$-GON-PEG was evaluated in PBS (pH 7.4 with 10 μM GSH, with the same procedure as the DOX-loaded $CPMAA_2$-GON-PEG).

The Korsmeyer-Peppas equation was used to analyze the release data to understand the release mechanism of the GON-based DDS, as given below:

$$M_t/M_\infty = k \cdot t^n \qquad (M_t/M_\infty < 0.6)$$

where M_t/M_∞ is the fraction of drug release at time t; k is a constant; and n is the release exponent.[39,40]

Cell Toxicity Assays. WST-1 assay was carried out to investigate the cytocompatibility of the $CPMAA_2$-GON-PEG nanocarriers and GON, cytotoxicity of the DOX-loaded $CPMAA_2$-GON-PEG nanocarriers, and DOX-loaded GON for SiHa cell and LSECs cell under typical conditions, as reported previously.[25]

Characterizations. The morphologies of the samples were characterized with a JEM-1200 EX/S transmission electron microscope (TEM) and a JSM-6380 scanning electron microscope (SEM). The unique structure of the PMAA-GON-PEG sample was revealed with a Bruker IFS 66 v/s infrared spectrometer. Fluorescence spectra of the DOX-loaded $CPMAA_2$-GON-PEG in deionized water and ethanol (2.5×10^{-4} mg mL^{-1}) were recorded with a FLS-920T fluorescence spectrophotometer at excitation wavelength of 485 nm. Thermogravimetric analysis (TGA) of the GON-PEG and PMAA-GON-PEG samples was obtained with a TA Instrument 2050 thermogravimetric analyzer at a heating rate of 10 °C min^{-1} from 25 to 600 °C at nitrogen atmosphere.

The drug loading and release performance was assessed using a PerkinElmer Lambda 35 UV−vis spectrometer (PerkinElmer Instruments, USA) at room temperature. DOX-loading capacity and loading efficiency were calculated by equations as follows:

$$\text{DOX} - \text{loading capacity (DLC)(mg mg}^{-1}) = \frac{\text{weight of DOX in nanocarriers}}{\text{weight of the nanocarriers}}$$

$$\text{DOX} - \text{loading efficiency (DLE) (\%)} = \frac{\text{weight of DOX in nanocarriers}}{\text{weight of the feeding DOX}} \times 100\%$$

The cumulative release (%) of drug at a particular time (t) was calculated as follows:

$$\text{Cumulative release (\%)} = \frac{C_t V_0 + V' \sum_{i=1}^{t-1} C_i}{M_{\text{total}}} \times 100\%$$

where M_{total} is the total content of DOX in dialysis tubes, V_0 and V' are the initial volume of release media and that at specific time intervals (here, V_0 = 120 mL and V' = 5 mL) respectively; C_t is the DOX concentration in release media at desired time t.

AUTHOR INFORMATION

Corresponding Author

*E-mail: pliu@lzu.edu.cn. Tel./Fax: 86-0931-8912582.

Notes

The authors declare no competing financial interest.

ACKNOWLEDGMENTS

This project was granted financial support from the National Nature Science Foundation of China (Grant no. 20904017), the Program for New Century Excellent Talents in University (Grant no. NCET-09-0441), the Fundamental Research Funds for the Central Universities (No. lzujbky-2014-245), and the National Science Foundation for Fostering Talents in Basic Research of the National Natural Science Foundation of China (Grant No. J1103307).

REFERENCES

(1) Novoselov, K. S., Geim, A. K., Morozov, S. V., Jiang, D., Zhang, Y., Dubonos, S. V., Grigorieva, I. V., and Firsov, A. A. (2004) Electric field effect in atomically thin carbon films. *Science 306*, 666−669.

DOI: 10.1021/bc5005137
Bioconjugate Chem. 2015, 26, 128−136

(2) Novoselov, K. S., Jiang, D., Schedin, F., Booth, T. J., Khotkevich, V. V., Morozov, S. V., and Geim, A. K. (2005) Two-dimensional atomic crystals. *Proc. Natl. Acad. Sci. U.S.A. 102*, 10451−10453.
(3) Geim, A. K. (2009) Graphene: Status and prospects. *Science 324*, 1530−1534.
(4) Goenka, S., Sant, V., and Sant, S. (2014) Graphene-based nanomaterials for drug delivery and tissue engineering. *J. Controlled Release 173*, 75−88.
(5) Chen, S., Hai, X., Xia, C., Chen, X. W., and Wang, J. H. (2013) Preparation of excitation-independent photoluminescent graphene quantum dots with visible-light excitation/emission for cell imaging. *Chem.—Eur. J. 19*, 15918−15923.
(6) Yang, K., Zhang, S., Zhang, G., Sun, X., Lee, S. T., and Liu, Z. (2010) Graphene in mice: Ultrahigh in vivo tumor uptake and efficient photo-thermal therapy. *Nano Lett. 10*, 3318−3323.
(7) Hu, W., Peng, C., Luo, W., Lv, M., Li, X., Li, D., Huang, Q., and Fan, C. (2010) Graphene-based antibacterial paper. *ACS Nano 4*, 4317−4323.
(8) Liu, J. Q., Cui, L., and Losic, D. (2013) Graphene and graphene oxide as new nanocarriers for drug delivery applications. *Acta Biomater. 9*, 9243−9257.
(9) Liu, Y., Yu, D., Zeng, C., Miao, Z., and Dai, L. (2010) Biocompatible graphene oxide-based glucose biosensors. *Langmuir 26*, 6158−6160.
(10) Singh, S. K., Singh, M. K., Kulkarni, P. P., Sonkar, V. K., Gracio, J. J. A., and Dash, D. (2012) Amine-modified graphene: Thrombo-protective safer alternative to graphene oxide for biomedical applications. *ACS Nano 6*, 2731−2740.
(11) Zhao, X. B., and Liu, P. (2014) Biocompatible graphene oxide as a folate receptor-targeting drug delivery system for the controlled release of anti-cancer drugs. *RSC Adv. 4*, 24232−24239.
(12) Yang, K., Wan, J. M., Zhang, S., Zhang, Y. J., Lee, S. T., and Liu, Z. (2011) *In vivo* pharmacokinetics, long-term biodistribution, and toxicology of PEGylated graphene in mice. *ACS Nano 5*, 516−522.
(13) Chen, M. L., He, Y. J., Chen, X. W., and Wang, J. H. (2013) Quantum-dot-conjugated graphene as a probe for simultaneous cancer-targeted fluorescent imaging, tracking, and monitoring drug delivery. *Bioconjugate Chem. 24*, 387−397.
(14) Chang, S. K., Bradley, D., Brian, C., and Vincent, M. R. (2013) Triggered nanoparticles as therapeutics. *Nano Today 8*, 439−447.
(15) Ge, Z. S., and Liu, S. Y. (2013) Functional block copolymer assemblies responsive to tumor and intracellular microenvironments for site-specific drug delivery and enhanced imaging performance. *Chem. Soc. Rev. 42*, 7289−7325.
(16) Gerweck, L. E., and Seetharaman, K. (1996) Cellular pH gradient in tumor versus normal tissue: Potential exploitation for the treatment of cancer. *Cancer Res. 56*, 1194−1198.
(17) Issels, R. D. (2008) Hyperthermia adds to chemotherapy. *Eur. J. Cancer 44*, 2546−2554.
(18) de la Rica, R., Aili, D., and Stevens, M. M. (2012) Enzyme-responsive nanoparticles for drug release and diagnostics. *Adv. Drug Delivery Rev. 64*, 967−978.
(19) Lee, E. S., Oh, K. T., Kim, D., Youn, Y. S., and Bae, Y. H. (2007) Tumor pH-responsive flower-like micelles of poly(L-lactic acid)-b-poly(ethylene glycol)-b-poly(L-histidine). *J. Controlled Release 123*, 19−26.
(20) Deng, C., Jiang, Y. J., Cheng, R., Meng, F. H., and Zhong, Z. Y. (2012) Biodegradable polymeric micelles for targeted and controlled anticancer drug delivery: Promises, progress and prospects. *Nano Today 7*, 467−480.
(21) Shi, S. X., Chen, F., Ehlerding, E. B., and Cai, W. B. (2014) Surface engineering of graphene-based nanomaterials for biomedical applications. *Bioconjugate Chem. 25*, 1609−1619.
(22) Chen, H., Wang, Z. Y., Zong, S. F., Wu, L., Chen, P., Zhu, D., Wang, C. M., Xu, S. H., and Cui, Y. P. (2014) SERS-fluorescence monitored drug release of a redox-responsive nanocarrier based on graphene oxide in tumor cells. *ACS Appl. Mater. Interfaces 6*, 17526−17533.
(23) Chen, Y., Xu, P. F., Shu, Z., Wu, M. Y., Wang, L. Z., Zhang, S. J., Zheng, Y. Y., Chen, H. R., Wang, J., Li, Y. P., et al. (2014) Multifunctional graphene oxide-based triple stimuli-responsive nano-theranostics. *Adv. Funct. Mater. 24*, 4386−4396.
(24) Feng, L. Z., Li, K. Y., Shi, X. Z., Gao, M., Liu, J., and Liu, Z. (2014) Smart pH responsive nanonanocarriers based on nano-graphene oxide for combined chemo- and photothermal therapy overcoming drug resistance. *Adv. Healthcare Mater. 3*, 1261−1271.
(25) Zhao, X. B., Liu, L., Li, X. R., Zeng, J., Jia, X., and Liu, P. (2014) Biocompatible graphene oxide nanoparticle-based drug delivery platform for tumor microenvironment-responsive triggered release of Doxorubicin. *Langmuir 30*, 10419−10429.
(26) Ma, L. J., Yang, X. M., Gao, L. F., Lu, M., Guo, C. X., Li, Y. W., Tu, Y. F., and Zhu, X. L. (2013) Synthesis and characterization of polymer grafted graphene oxide sheets using a Ce(IV)/HNO_3 redox system in an aqueous solution. *Carbon 53*, 269−276.
(27) Yagci, C., and Yildiz, U. (2005) Redox polymerization of methyl methacrylate with allyl alcohol 1,2-butoxylate-block-ethoxylate initiated by Ce(IV)/HNO_3 redox system. *Eur. Polym. J. 41*, 177−184.
(28) Derkaoui, S. M., Avramoglou, T., Barbaud, C., and Letourneur, D. (2008) Synthesis and characterization of a new polysaccharide-graft-polymethacrylate copolymer for three-dimensional hybrid hydrogels. *Biomacromolecules 9*, 3033−3038.
(29) Go, Y. M., and Jones, D. P. (2008) Redox compartmentalization in Eukaryotic cells. *Biochim. Biophys. Acta, Gen. Subj. 1780*, 1271−1290.
(30) Söderholm, K. J. M., and Shang, S. W. (1993) Molecular orientation of silane at the surface of colloidal silica. *J. Dent. Res. 72*, 1050−1054.
(31) Pan, Y. Z., Bao, H. Q., Sahoo, N. G., Wu, T. F., and Li, L. (2011) Water-soluble poly(N-isopropylacrylamide)−graphene sheets synthesized via click chemistry for drug delivery. *Adv. Funct. Mater. 21*, 2754−2763.
(32) Shen, J., Hu, Y., Li, C., Qin, C., and Ye, M. (2009) Synthesis of amphiphilic graphene nanoplatelets. *Small 5*, 82−85.
(33) Sun, X. M., Liu, Z., Welsher, K., Robinson, J. T., Goodwin, A., Zaric, S., and Dai, H. J. (2008) Nano-graphene oxide for cellular imaging and drug delivery. *Nano Res. 1*, 203−212.
(34) Yang, X. Y., Zhang, X. Y., Liu, Z. F., Ma, Y. F., Huang, Y., and Chen, Y. S. (2008) High-efficiency loading and controlled release of Doxorubicin hydrochloride on graphene oxide. *J. Phys. Chem. C 112*, 17554−17558.
(35) Raval, A., Parikh, J., and Engineer, C. (2011) Mechanism and *in vitro* release kinetic study of sirolimus from a biodegradable polymeric matrix coated Cardiovascular Stent. *Ind. Eng. Chem. Res. 50*, 9539−9549.
(36) Franson, N. W., and Peppas, N. A. (1983) Influence of copolymer composition on non-fickian water transport through glassy copolymers. *J. Appl. Polym. Sci. 28*, 1299−1310.
(37) Kim, T. H., Park, I. K., Nah, J. W., Choi, Y. J., and Cho, C. S. (2004) Galactosylated chitosan/DNA nanoparticles prepared using water-soluble chitosan as a gene carrier. *Biomaterials 25*, 3783−3792.
(38) Hummers, W. S., and Offeman, R. E. (1958) Preparation of graphitic oxide. *J. Am. Chem. Soc. 80*, 1339−1339.
(39) Korsmeyer, R. W., Gurny, R., Doelker, E. M., Buri, P., and Peppas, N. A. (1983) Mechanism of solute release from porous hydrophilic polymers. *Int. J. Pharm. 15*, 25−35.
(40) Siepmann, J., and Peppas, N. A. (2001) Modeling of drug release from delivery systems based on hydroxypropyl methylcellulose (HPMC). *Adv. Drug Delivery Rev. 48*, 139−157.

DOI: 10.1021/bc5005137
Bioconjugate Chem. 2015, 26, 128−136